Promoting liver cancer cell apoptosis effect of *Tribulus terrestris* L. via reducing sphingosine level was confirmed by network pharmacology with metabolomics☆

Jing Zhao [a], Jia-Qi Zhang [a], Tan-Tan Li [a], Sen Qiao [b,*], Shu-Long Jiang [a,**]

[a] *Clinical Medical Laboratory Center, Jining No.1 People's Hospital, Shandong First Medical University, Jining, China*
[b] *Hepatological Surgery Department, Jining No.1 People's Hospital, Shandong First Medical University, Jining, China*

ABSTRACT

Background: Tribulus terrestris L. (TT) is one of the most common Chinese herbs and distributes in various regions in China. TT was first documented to treat breast cancer in Shen-Nong-Ben-Cao-Jing. However, the pharmacological activities of TT extract on liver cancer have not been reported. In this study, we investigated its anti-liver cancer activity and underlying mechanism.
Methods: Traditional Chinese Medicine Systems Pharmacology (TCMSP) and PharmMapper databases were used to obtain the active ingredients and the targets of TT. Genecards database was employed to acquire TT targets in liver cancer. Furthermore, Venny 2.1, Cytoscape 3.8.2, DAVID 6.8 software were utilized to analyze the relationship between TT and liver cancer. *In vivo* **experiment**: The animal model of liver cancer was established by injection of H22 cells into Balb/c mice. After five days, drugs were intragastrically administered to the mice daily for 10 days. Body weight, tumor size and tumor weight were recorded. Tumor inhibitory rate was calculated. Protein levels were examined by Western blotting. Pathological changes of liver cancer tissues were evaluated by HE and Tunel staining. **Metabolomics study:** LC-MS was used to analyze different metabolites between model and TTM groups.
Results: 12 active ingredients of TT, 127 targets of active ingredients, 17,378 targets of liver cancer, and 125 overlapping genes were obtained. And then, 118 items of GO biological processes (BP), 54 items of GO molecular function (MF), 35 items of GO cellular component (CC) and 128 pathways of KEGG were gotten ($P < 0.05$). Moreover, 47 differential metabolites were affirmed and 66 pathways of KEGG ($P < 0.05$) were obtained. In addition, after TT and sorafenib treatment, tumor size was markedly reduced, respectively, compared with model group. Tumor weight was significantly decreased and tumor inhibitory rate was more than 44% in TTM group. After TT treatment, many adipocytes, cracks between tumor cells and apoptosis were found. The levels of pro-Cathepsin B, Cathepsin B, Bax, Bax/Bcl2, Caspase3 and Caspase7 were markedly increased, but the level of Bcl2 was significantly reduced after TT treatment.
Conclusion: TT has a broad range of effects on various signaling pathways and biological processes, including the regulation of apoptosis. It exhibits antitumor activity in an animal model of liver cancer and activates the apoptotic pathway by decreasing Sph level. This study provides

valuable information regarding the potential use of TT extract in the treatment of liver cancer and highlights the importance of investigating the underlying molecular mechanisms of traditional medicines for the development of new therapeutic drugs in liver cancer.

1. Introduction

Liver cancer is a common malignant tumor worldwide. According to the report of International Agency for Research on Cancer (IARC) in 2020, China had the highest morbidity and mortality of liver cancer compared with the rest world [1]. There were 0.91 million new liver cancer patients and 0.83 million deaths around the world in 2020. However, 0.41 million new patients and 0.39 million deaths were in China. In addition, there were higher morbidity or mortality in men than women. Liver cancer is divided into primary and secondary liver cancer. Primary liver cancer (PLC) is that cancer cells originate from the epithelial and mesenchymal tissue of liver and its morbidity accounts for 90% of liver cancer. Previous studies found that hepatocarcinogenesis, especially PLC, was a complex process induced by many factors, including hepatitis B virus, hepatitis C virus, aflatoxin and liver cirrhosis [2–4]. Clinically surgery is the first choice for early PLC because it provides only chance for cure but has limited applicability. Adjuvant therapy, including chemotherapy, radiation and targeted therapy, are used for advanced PLC patients. In addition, accumulated studies showed that traditional Chinese medicine (TCM) is an alternative treatment for PLC because of its effective therapeutic outcome and fewer side effects compared to chemo-radiotherapy [5,6]. For example, Bei-Jia-Jian-Wan and Xiao-Chai-Hu-Tang are two of the most frequently used Chinese herbal medicine for PLC. Other TCMs used for PLC include *Hedyotis diffusea* Willd. (Bai-Hua-She-She-Cao), *Scutellaria barbata* D. Don (Ban-Zhi-Lian), *Salvia miltiorrhiza Bge* (Dan-shen), *Brucea javanica* (L.). Merr. (Ya-Dan-Zi) and *Iphigenia indica* Kunth (Shan-Ci-Gu) [5–7].
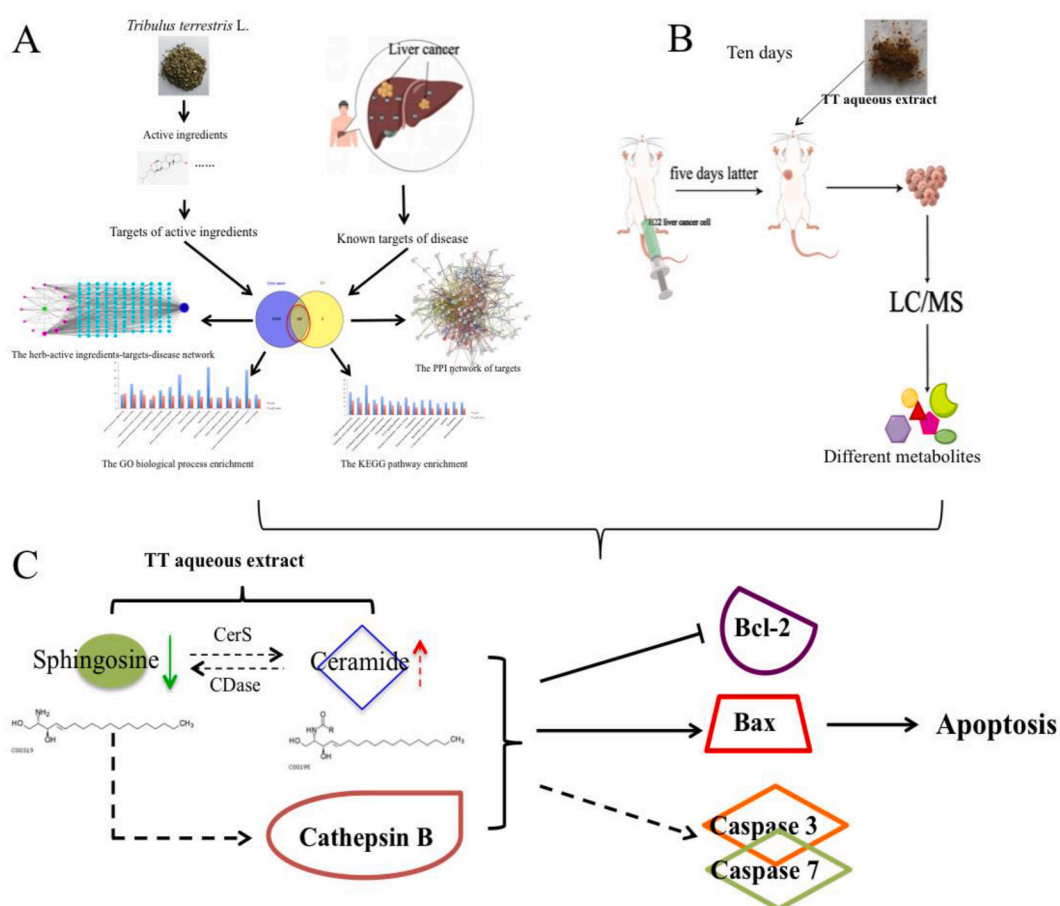
Fig. 1. The design of this study. Illustration of experimental workflow: (A) Network pharmacology study of TT's anti-liver cancer effect including targets collection, construction of Herb-Ingredients-Targets-Disease network and PPI network, GO and KEGG pathway analysis. (B) Metabonomics study of TT's anti-liver cancer effect. (C) Descriptive and correlational analysis between sphingosine and apoptosis induced by TT. The partial figure was drawn by Figdraw software (http://www.figdraw.com/static/index.html#/).

Based on TCM theory, *Tribulus terrestris* L. (TT), a common herb and first documented in Shen-Nong-Ben-Cao-Jing, is able to calm liver and dispel melancholy ("Ping Gan Jie Yu in Chinese), promote blood circulation to dissipate wind ("Huo Xue Qu Feng" in Chinese), improve eyesight ("Ming Mu" in Chinese) and relieve itching ("Zhi Yang" in Chinese). Previous studies demonstrated the effects of TT on prostate health [8], reproductive processes [9], hypertensive renal injury [10], inflammation, ovarian cells apoptosis and so on [11]. But the study on anti-liver cancer of TT was hardly reported. According to pathogenic factors and pathogenesis of TCM, liver cancer were divided into different syndromes including stagnation of liver-qi and deficiency of spleen ("Gan Yu Pi Xu" in Chinese), stagnated vital energy clots the blood ("Qi Zhi Xue Yu" in Chinese), cold-dampness obstructing the spleen ("Han Shi Kun Pi" in Chinese), yin deficiency of liver and kidney ("Gan Shen Yin Xu" in Chinese) [12]. Thus we speculated that there were close relations between liver cancer and TT because of its TCM effects.

In this study, we demonstrated the anti-liver cancer effect of TT *in vivo* with effectiveness equivalent to even better than sorafinib. Additionally, we investigated the underlying molecular mechanisms of TT's anti-tumor effects using network pharmacology and metabolomics (Fig. 1) and found the apoptotic pathway as a major target of TT in PLC. Overall, our study provides important insights into the potential use of TT as a therapeutic drug for PLC and highlights the importance of using multi-disciplinary approaches to investigate the mechanisms of action of traditional medicines like TT.

2. Materials and methods

2.1. Network pharmacology study

2.1.1. Screening of major active ingredients of TT and collection of potential targets

The major active ingredients of TT were gotten from the Traditional Chinese Medicine Systems Pharmacology (TCMSP) database (https://tcmsp-e.com/). Screening parameters were set with Oral bioavailability (OB) greater than or equivalent to 30% and drug-likeness (DL) greater than or equivalent to 0.18. The potential targets of the major active ingredients were obtained from the TCMSP and PharmMapper database (Norm Fit>0.9, http://www.lilab-ecust.cn/pharmmapper/), which was used as a supplement for targets prediction. Subsequently, the information of acquired targets was standardized by Uniprot database (https://www.uniprot.org/).

2.1.2. Targets collection of TT on liver cancer

The targets of liver cancer were gotten from Genecards database (https://www.genecards.org/) using "Homo sapiens" as species and "liver cancer" as keywords. In addition, the targets of drug and disease were mapped by Venny 2.1 online software (https://bioinfogp.cnb.csic.es/tools/venny/) to predict potential targets of TT on liver cancer.

2.1.3. Construction of herb-ingredients-targets-disease network and protein-protein interaction (PPI) network

The Herb-Ingredients-Targets-Disease network was constructed by using Cytoscape 3.8.2 software. PPI network was constructed by using String 11.0 online software (https://www.string-db.org/) and Cytoscape 3.8.2 software.

2.1.4. Enrichment analysis of GO and KEGG pathway

The enrichment analysis of gene ontology (GO) and Kyoto Encyclopedia of Genes and Genomes (KEGG) pathway were conducted by DAVID 6.8 online software (https://david.abcc.ncifcrf.gov/).

2.2. In vivo experiment

2.2.1. TT aqueous extract

TT was purchased from Jining Banger Chinese Herbal Medicine Co. Ltd. (Jining, Shandong, China) and morphologically authenticated by Professor Hong-Jie Liu at Jinan university. The quality of TT met the requirements of Chinese pharmacopoeia (2020).

The raw TT was separately reflux-extracted thrice with 10-fold volume of distilled water for 1 h. The combined extracts were filtered, concentrated and then lyophilized with a Virtis Freeze Dryer (Qingdao creatrust electronic technology Co., Ltd., Qingdao, Shandong, China). The resulting extracts were weighed and the yield was calculated (TT yield: 16%). These crude extracts were conserved at 4 °C for further use. Tribuloside D was quantified to control the quality of the TT aqueous extract. HPLC analysis of TT aqueous extract showed tribuloside D content of 0.072 mg/g. The detailed information was described in our other study.

2.2.2. H22 liver cancer mice model and experimental design

Male Balb/c mice (SPF, certificate number SCXK (Lu) 20190003), weighing 16–18 g, were purchased from Jinan pengyue laboratory animal breeding Co., Ltd. Mice were kept in the animal facility at clinical medical laboratory center under standard conditions at 21–23 °C with a relative humidity of 50–60%. All experimental procedures were approved by the University Committee on Research Practice in Jining No.1 People's Hospital (No.: JNRM-2021-DW-050).

After adaptive breeding for five days, 50 mice were subcutaneously injected with 5×10^6 cells/mL $\times$ 100 μL H22 cells in left subaxillary region. After five days, mice were randomly divided into model group, sorafenib group, TT high dose (TTH) group, TT medium dose (TTM) group, TT low dose (TTL) group, ten mice in each group. Mice in sorafenib group were treated with sorafenib (20 mg/kg), while mice in TT groups were treated with TT aqueous extract (0.84 g/kg, 0.42 g/kg, 0.21 g/kg) for ten days by oral administration.

During the experiment, body weight and tumor size ($V = 0.52 \times \text{length} \times \text{width}^2$, cm^3) were recorded once three or four days. At the end of the trial, tumor weight was recorded, tumor inhibitory rate was calculated by (W$_{\text{model group}}$-W$_{\text{drug group}}$)/W$_{\text{model group}}$ × 100%, and then liquid nitrogen quick freezing tumor tissues were selected for metabonomics and Western blot. Finally, the tumor tissue was fixed in 4% paraformaldehyde for Hematoxylin and eosin (HE) staining and Tunel staining.

2.2.3. HE staining
The tumor tissue was fixed in 4% paraformaldehyde and then embedded in paraffin. The paraffin block was cut into 5 μm thick slices. HE staining was performed as described [13].

2.2.4. Tunel staining
The paraffin block was cut into 5 μm thick slices and then stained with Tunel staining according to the manufacturer's protocol. The kit was purchased from Beyotime Biotechnology (Shanghai, China).

2.2.5. Western blot analysis
Western blot analysis was performed as previously described [14]. The expression level of apoptosis-related proteins, including pro-cathepsin B, cathepsin B, Bax, Bcl2, caspase3 and caspase7 in tumor tissue, were detected with Western blot. In addition, the level of GAPDH in tumor was detected as control for quantitative analysis.

Tumor tissues were homogenized in RIPA buffer and 1 mM phenylmethylsulfonyl fluoride and then incubated on ice for 0.5 h. Proteins were gotten by centrifuging at 14,000 g at 4 °C for 15 min and quantified using the Beyotime protein assay regent. And then, equal amounts of proteins (20 μg) mixed with loading buffer were denatured, separated, transferred membrane, blocked, incubated with primary and secondary antibodies, detected using ECL reagents. In the last, relative protein expression level was analyzed using IPP software.

2.2.6. Statistical analysis
Results were presented as mean ± SEM. Data between multiple groups were analyzed by one-way analysis of variance (ANOVA) using SPSS (version 20.0) statistical analysis program, and then differences among means were analyzed using Dunnett's multiple comparisons test or post hoc analysis. Differences were considered significant at $P < 0.05$.

2.3. Metabonomics of tumor tissue

2.3.1. Sample preparation
Tumor tissue in model and TTM groups were chosen for metabonomics (N = 5).

1 mL of cold extraction solvent methanol/acetonitrile/H2O (2:2:1, v/v/v) was added to80 mg sample, and adequately vortexed. The lysate was homogenized by MP homogenizer and sonicated at 4 °C (30 min × 2) then centrifuged at 14,000 g for 20 min at 4 °C and the supernatant was dried in a vacuum centrifuge at 4 °C. For LC-MS analysis, the samples were re-dissolved in 100 μL acetonitrile/water (1:1, v/v) solvent.

2.3.2. LC-MS, data and Bioinformatics analysis
For untargeted metabolomics of polar metabolites, extracts were analyzed using a quadrupole time-of-flight mass spectrometer (Sciex Triple TOF 6600) coupled to hydrophilic interaction chromatography via electrospray ionization in Shanghai Applied Protein Technology Co., Ltd. LC separation was on a ACQUIY UPLC BEH Amide column (2.1 mm × 100 mm × 1.7 μm, waters) using a gradient of solvent A (25 mM ammonium acetate and 25 mM ammonium hydroxide in water) and solvent B (acetonitrile). The gradient was 0–0.5 min: 5%A:95%B; 0.5–7 min: 5%A:95%B to 35%A:65%B; 7–8 min: 35%A:65%B to 60%A:40%B; 8–9 min: 60%A:40%B; 9–9.1 min: 60%A:40%B to 5%A:95%B; 9.1–12 min: 5%A:95%B. Flow rate was 0.5 mL/min, column temperature was 25 °C, auto sampler temperature was 4 °C, and injection volume was 2 μL.

The mass spectrometer was operated in both negative ionizations and positive ionizations mode. The ESI source conditions were set as follows: Ion Source Gas1 (Gas1) as 60, Ion Source Gas2 (Gas2) as 60, curtain gas (CUR) as 30 psi, source temperature: 600 °C, Ion Spray Voltage Floating (ISVF) ±5500 v. In MS acquisition, the instrument was set to acquire over the m/z range 60–1000 Da, and the accumulation time for TOF MS scan was set at 0.20 s/spectra. In auto MS/MS acquisition, the instrument was set to acquire over the m/z range 25–1000 Da, and the accumulation time for product ion scan was set at 0.05 s/spectra. The product ion scan is acquired using information dependent acquisition (IDA) with high sensitivity mode selected. The parameters were set as follows: the collision energy (CE) was fixed at 35 ± 15 eV; declustering potential (DP), 60 V (+) and −60 V (−); exclude isotopes within 4 Da, candidate ions to monitor per cycle: 10.

The raw MS data were converted to MzXML files using ProteoWizard MS Convert before importing into freely available XCMS software. For peak picking, the following parameters were used: centWave $m/z = 25$ ppm, peakwidth = c (10, 60), prefilter = c (10, 100). For peak grouping, bw = 5, mzwid = 0.025, minfrac = 0.5 were used. In the extracted ion features, only the variables having more than 50% of the nonzero measurement values in at least one group were kept. Compound identification of metabolites by MS/MS spectra with an in-house database established with available authentic standards. After normalized to total peak intensity, the processed data were uploaded into before importing into SIMCA-P (version 14.1, Umetrics, Umea, Sweden), where it was subjected to multivariate data analysis, including Pareto-scaled principal component analysis (PCA) and orthogonal partial least-squares

Table 1
The information of TT's active ingredients.

	Molecule Name	MW (Da)	OB (%)	DL	AlogP	Hdon	Hacc	Caco-2	BBB	FASA-	HL
TT1	isorhamnetin	316.28	49.60	0.31	1.755	4	7	0.31	−0.54	0.32	14.34
TT2	sitosterol	414.79	36.91	0.75	8.084	1	1	1.32	0.87	0.22	5.37
TT3	kaempferol	286.25	41.88	0.24	1.771	4	6	0.26	−0.55	0	14.74
TT4	(Z)-3-(4-hydroxy-3-methoxy-phenyl)-N-[2-(4-hydroxyphenyl)ethyl]acrylamide	313.38	118.35	0.26	2.859	3	5	0.51	−0.27	0	4.26
TT5	(2aR,2′R,4R,6aR,6bS,8aS,8bR,11aS,12aR,12bR)-4-((S)-2-(2,6-dimethylphenyl)propoxy)-5′,5′,6a,8a-tetramethyl-8-methylenedocosahydro-1H-spiro[pentaleno [2,1-a]phenanthrene-10,2′-pyran]	573	59.49	0.28	9.376	0	2	1.49	0.78	0.26	7.16
TT6	(3R,8S,9S,10R,13R,14R,17S)-17-((2S,5R)-5-ethyl-6-methylheptan-2-yl)-3-hydroxy-10,13-dimethyl-3,4,8,9,10,11,12,13,14,15,16,17-dodecahydro-1H-cyclopenta[a]phenanthren-7(2H)-one	428.77	40.93	0.79	7.153	1	2	0.76	0.12	0.27	3.00
TT7	(3R,7R,8S,9S,10S,13R,14S,17R)-17-((2R,5S)-5-ethyl-6-methylheptan-2-yl)-3,10-dimethyl-2,3,4,7,8,9,10,11,12,13,14,15,16,17-tetradecahydro-1H-cyclopenta[a]phenanthren-7-ol	414.79	34.21	0.76	8.332	1	1	1.34	1.00	0.22	4.58
TT8	(Z)-3-(3,4-dihydroxyphenyl)-N-[2-(4-hydroxyphenyl)ethyl]acrylamide	299.35	113.25	0.24	2.608	4	5	0.41	−0.35	0.39	4.87
TT9	β-sitosterol-β-D-glucopyranoside	398.79	32.41	0.71	9.117	0	0	1.86	1.86	0.23	4.12
TT10	terrestriamide	327.36	114.09	0.29	2.424	3	6	0.18	−0.60	0.37	19.05
TT11	(2aR,2′S,4R,4′R,5′S,6aS,6bS,8aS,8bR,9S,11aR,12aR,12bR)-4,4′-dihydroxy-5′,6a,8a,9-tetramethylicosahydro-1H-spiro[pentaleno [2,1-a]phenanthrene-10,2′-pyran]-8(2H)-one	444.72	58.74	0.76	3.265	2	4	0.05	−0.70	0.21	4.77
TT12	(2aR,5S,6aS,6bS,8aS,8bS,11aS,12aR,12bR)-10-isopentyl-6a,8a,9-trimethyl-2,2a,3,4,5,6,6a,6b,7,8,8a,8b,11a,12,12a,12b-hexadecahydro-1H-naphtho[2′,1':4,5]indeno [2,1-b]furan-5-ol	400.71	39.21	0.84	5.931	1	2	1.21	0.82	0.21	4.39

discriminant analysis (OPLS-DA). The 7-fold cross-validation and response permutation testing were used to evaluate the robustness of the model. The variable importance in the projection (VIP) value of each variable in the OPLS-DA model was calculated to indicate its contribution to the classification. Significance was determined using an unpaired Student's *t*-test. VIP value > 1 and $P < 0.05$ was considered as statistically significant.

For KEGG pathway annotation, the metabolites were blasted against the online Kyoto Encyclopedia of Genes and Genomes (KEGG) database to retrieve their Cos and were subsequently mapped to pathways in KEGG11. The corresponding KEGG pathways were extracted. To further explore the impact of differentially expressed metabolites, enrichment analysis was performed. KEGG pathway enrichment analyses were applied based on the Fisher' exact test, considering the whole metabolites of each pathway as background dataset. And only pathways with *P*-values under a threshold of 0.05 were considered as significant changed pathways.

3. Results

3.1. Screening of major active ingredients of TT and action target results

In this study, 12 active ingredients were gotten from TCMSP database with the values of OB and DL greater than or equivalent to 30% and 0.18, respectively. The information of active ingredients was displayed in Table 1. We found 127 targets by using TCMSP and PharmMapper database, 37 of which were from TT1, 3 from TT2, 62 from TT3, 8 from TT4, 16 from TT5, 27 from TT6, 25 from TT7, 49 from TT8, 18 from TT9, 5 from TT10, 1 from TT11, 4 from TT12. The target results were seen in Fig. 2B.
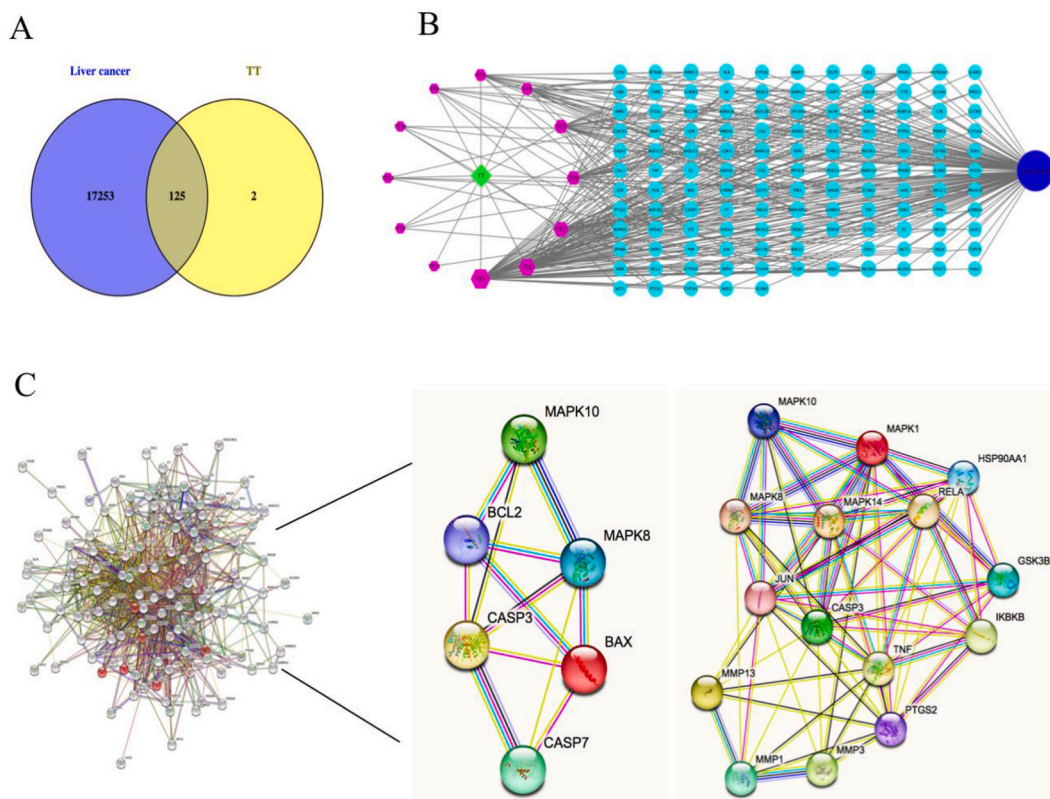

Fig. 2. Network construction between TT and liver cancer. (A) Potential targets of TT's active ingredients in the treatment of liver caner. Purple circle represents targets of liver cancer. Yellow circle represents targets of TT. There were 125 overlapping genes between liver cancer and TT. (B) The construction of herb-active ingredients-targets-disease network. Green node represents TT. Purple nodes represent the active ingredients of TT. Sky blue nodes represent the intersecting targets between herb and disease. Dark blue node represents liver cancer. (C) Protein-protein interaction (PPI) network of intersecting targets of core ingredients and liver cancer. Empty node represents a protein of unknown 3D structure. Filled nodes represent proteins of known or predicted 3D structures. Sky-blue lines represent known interactions from curated databases. Purplish red lines represent known interaction experimentally determined. Grass green lines represent the predicted interaction of gene neighborhood. Red lines represent the predicted interaction of gene fusion. Dark blue lines represent the predicted interaction of gene co-occurrence. Light green lines represent the relationship of textmining. Black lines represent the relationship of co-expression. Purple lines represent the relationship of protein homology. (For interpretation of the references to color in this figure legend, the reader is referred to the Web version of this article.)

3.2. Prediction of potential targets of TT's active ingredients in liver cancer treatment

17,378 targets about liver cancer were gotten from Genecards database. The result of potential targets of TT's ingredients in liver cancer was shown in Fig. 2A. Fig. 2A showed that the total of 125 targets in the treatment of liver cancer were found by Venny 2.1 online software. For example, EGFR, AKT1, ESR1, AR, PPARG etc.

3.3. The herb-ingredients-targets-disease network and PPI network

The herb-ingredients-targets-disease network (as shown in Fig. 2B) was constructed with Cytoscape 3.8.2 software. There were 139 nodes in this network, which revealed the relationships between active ingredients and the targets were visually shown in this network. For example, the potential therapeutic targets of TT1 included NOS2, PTGS1, PTPN1, ESR2, DPP4, MAPK14 etc.; targets of TT2 included NCOA2, NR3C2, PGR; targets of TT3 included NOS2, PTGS1, AR, PPARG, PTGS2, PIK3CG etc.

We also estimated the importance of ingredients and targets by the size of symbol, and there was a positive correlation between them. Such as the size of TT3 symbol was the biggest in all active ingredients, implaying that TT3 had the most potential therapeutic targets and was the most important.

In addition, the PPI network (as shown in Fig. 2C) was constructed with String 11.0 online software. There were 125 nodes (representing proteins) and 1039 edges (representing the interactions between the proteins) in this network. The average node degree of the target proteins was 16.6. The relevant degree among those proteins were shown in this network, such as CASP7 had relationships with BAX, PPP3CA, CTSV etc.; BCL2 had relationships with MAPK10, CDK2 etc.

3.4. Analysis on GO and KEGG pathway of targets

The GO function enrichment analysis was carried out by DAVID 6.8 online software to obtain 118 items of biological processes (BP)
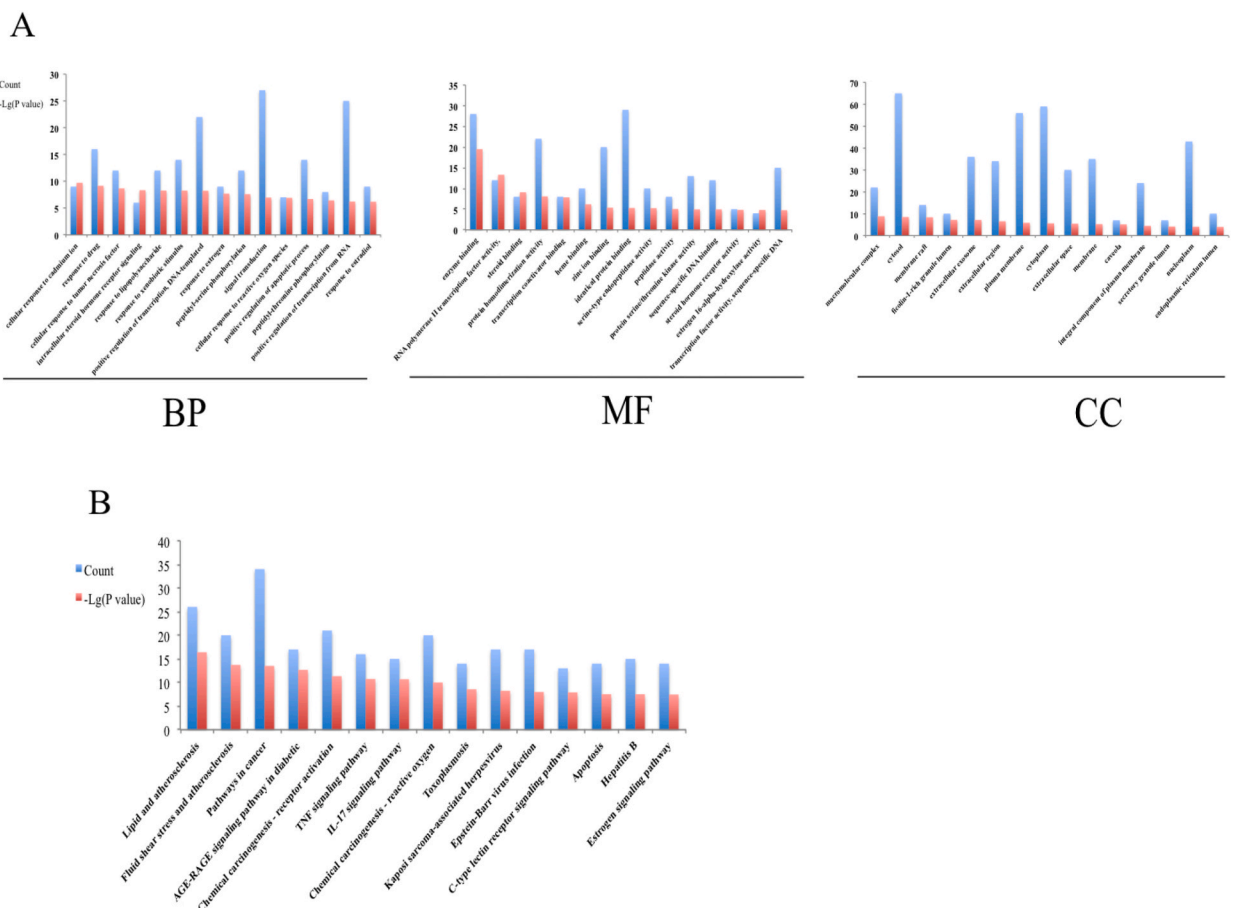

Fig. 3. Data enrichment analysis of network pharmacology. (A) Gene Ontology (GO) analysis of intersecting targets. BP represents GO biological processes enrichment analysis. MF represents GO molecular functions enrichment analysis. CC represents GO cellular components enrichment analysis. (B) KEGG analysis of intersecting targets.

($P < 0.05$)/54 items of molecular function (MF) ($P < 0.05$), 35 items of cellular component (CC) ($P < 0.05$), the top 15 items were shown in Fig. 3A. The target enrichment was relatively concentrated in the BP, for example cellular response to cadmium ion; response to drug; cellular response to tumor necrosis factor; response to lipopolysaccharide; response to xenobiotic stimulus; positive regulation of transcription, DNA-templated; response to estrogen; peptidyl-serine phosphorylation; signal transduction; cellular response to reactive oxygen species; positive regulation of apoptotic process etc. It revealed that TT could regulate the changes in many biological pathways caused by liver cancer. The detailed information of BP, MF and CC results was seen in Supplementary results.

In addition, 128 pathways were screened from KEGG pathway enrichment ($P < 0.05$) by using DAVID 6.8 online software. The top 15 pathways were shown in Fig. 3B. Target genes were enriched in these pathways, some of which were related to liver cancer, including Pathways in cancer, TNF signaling pathway, IL-17 signaling pathway, Apoptosis etc. The results revealed that TT might have therapeutic effects on liver cancer through anti-inflammation, anti-apoptosis etc. The detailed information of KEGG pathway enrichment results was seen in Supplementary results.

3.5. Effects of TT on H22 liver cancer mice

After TT and sorafenib treatment for 10 days, changes of body weight were not significant, but tumor weight in TTM group was markedly decreased compared with model group (Fig. 4A–B). After drug treatment, tumor inhibitory rates were above 20%, especially tumor inhibitory rate was more than 44% in TTM group (Fig. 4C). Moreover, Fig. 4D showed that after 3, 6, 10 days of TT and sorafenib treatment, tumor size was markedly reduced, respectively, compared with model group.
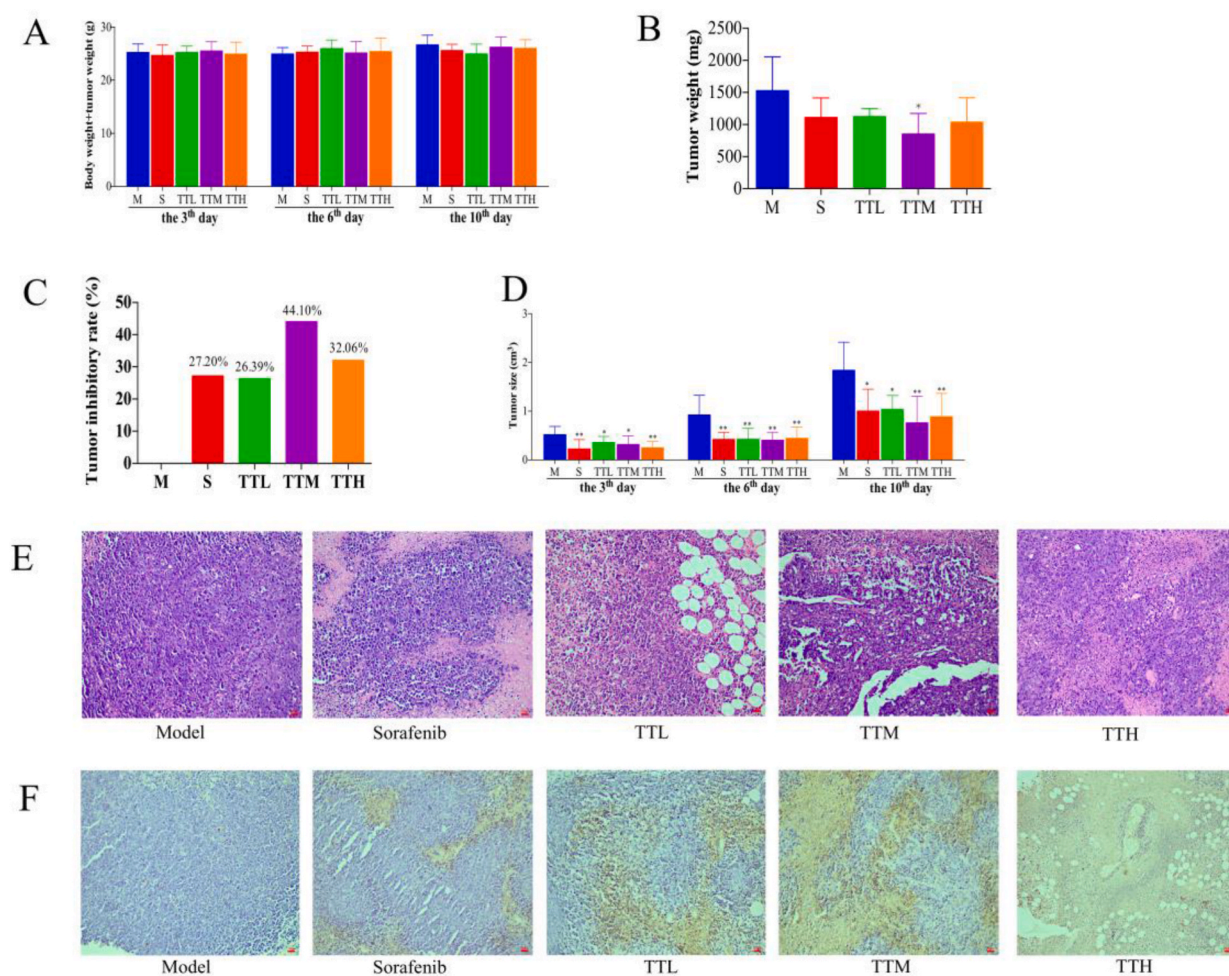

Fig. 4. Effects of TT on H22 liver cancer mice. (A) Effect of TT on body weight. (B) Effects of TT on tumor weight. (C) Effects of TT on tumor inhibitory rate. Tumor inhibitory rate was calculated by ($W_{model\ group}$-$W_{drug\ group}$)/$W_{model\ group}$ × 100%. (D) Effect of TT on tumor size. Tumor size was calculated by $0.52 \times length \times width^2$. (E) Effect of TT on tumor tissue pathology. Tumor pathological changes were evaluated by hematoxylin and eosin (HE) staining (20 ×). (F) Effect of TT on tumor tissue apoptosis. Apoptosis was evaluated by Tunel staining (20 ×). Values given are the mean ± SEM. *$P < 0.05$, **$P < 0.01$ versus model group. Statistical significant differences were determined using a one-way ANOVA followed by Dunnett's multiple comparisons test or post hoc analysis.

Effects of TT on tumor tissue pathology were shown in Fig. 4E. In model group, tumor cells were tightly arranged; the boundary between cells lacked sharpness; the adenoid structure, hyperchromatic and pleomorphic tumor cell nucleus were found. Moreover, cell nucleus fragments were found after sorafenib treatment. In addition, cell nucleus fragments, adipocyte and cracks between tumor cells were discovered after TT treatment.

Effects of TT on apoptosis were shown in Fig. 4F. Tumor cell apoptosis was evaluated by Tunel stains, and only apoptotic cell was stained with yellowish-brown. There was a few apoptotic cells in model group. Moreover, a large of apoptotic cells were decreased after sorafenib and TT treatment.

3.6. Multivariate statistical analysis of metabolites

1653 metabolites (positive polarity mode: 1043; negative polarity mode: 610) were identified in this untargeted metabolomics. The orthogonal partial least-squares discriminant analysis (OPLS-DA) scores plot showed that there was an excellent discrimination between the model and the TT group as shown in Fig. 5A. And then, permutation test were executed to ensure the validity of relation between the model and the TT group as shown in Fig. 5B. The parameters of permutation test indicated that there was a clearly separation between the model and the TT group in negative polarity mode ($R^2X = 0.521$, $R^2Y = 0.995$, $Q^2 = 0.482$) and positive polarity mode ($R^2X = 0.596$, $R^2Y = 0.992$, $Q^2 = 0.661$).

3.7. Affirmation of differential metabolites

47 differential metabolites were affirmed according to VIP >1 and P-value <0.05 (Data were shown in Fig. 5C) in model and TT groups. There were 5 up-regulated and 4 down-regulated metabolites in negative polarity mode. Moreover, there were 11 up-regulated and 27 down-regulated metabolites in positive polarity mode. The detailed information of differential metabolites was seen in Table 2.

3.8. Functional analysis of differential metabolites

The hierarchical clustering analysis results of differential metabolites were shown by heat-map. Fig. 6A showed an expressive tendency of differential metabolites in model and TT groups, as well as affinity degrees of metabolites. Metabolites, which in the same cluster had similar expression mode, might have alike function or participate in the same metabolic process or cellular pathway. For example, sphingosine, benzalkonium chloride (c12) and tetradecylamine were low-expression in TT group but high-expression in model group.

Correlation analysis was done to understand the interaction of differential metabolites in the process of biological state change. Correlation analysis results showed the relationship between single metabolite and the other (Fig. 6B). For example, sphingosine was closely related to 1-palmitoylglycerol, benzalkonium chloride (c12), tetradecylamine and lauryldimethylamine oxide.
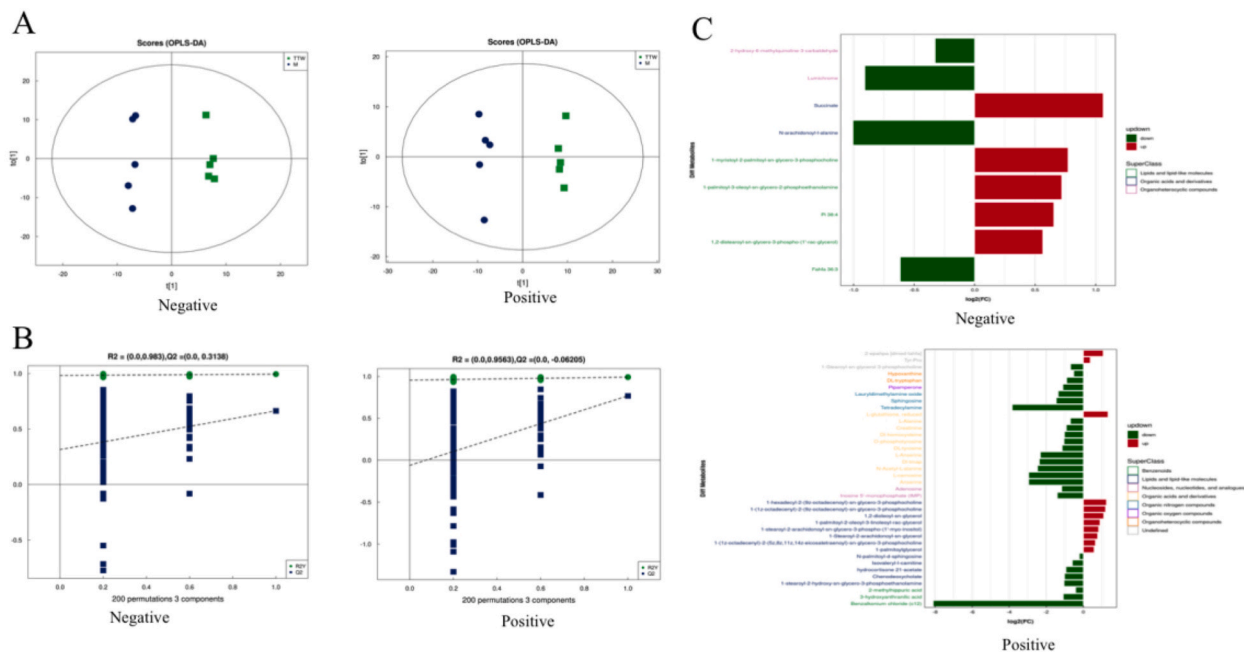

Fig. 5. Quality control of metabonomics and differential metabolites. (A) The orthogonal partial least-squares discriminant analysis (OPLS-DA) scores. (B) Permutation test for OPLS-DA. (C) Differential metabolites and their superclass.

Table 2
The detailed information of different metabolites.

ID	Adduct	Name	VIP	Fold change	P-value	m/z	SuperClass
M751T40	[M + HCO2]-	1-myristoyl-2-palmitoyl-*sn*-glycero-3-phosphocholine	3.25	1.71	0.012	750.54	Lipids and lipid-like molecules
M374T35	[M − H]-	N-arachidonoyl-L-alanine	3.81	0.50	0.013	374.25	Organic acids and derivatives
M717T152	[M − H]-	1-palmitoyl-3-oleoyl-*sn*-glycero-2-phosphoethanolamine	2.55	1.65	0.017	716.52	Lipids and lipid-like molecules
M117T90	[M − H]-	Succinate	3.80	2.09	0.017	117.02	Organic acids and derivatives
M241T62	[M − H]-	Lumichrome	3.55	0.53	0.026	241.07	Organoheterocyclic compounds
M886T195	[M − H]-	Pi 38:4	10.06	1.57	0.026	885.55	Lipids and lipid-like molecules
M186T231_1	[M − H]-	2-hydroxy-6-methylquinoline-3-carbaldehyde	3.43	0.80	0.029	186.05	Organoheterocyclic compounds
M559T40	[M − H]-	Fahfa 36:3	1.35	0.65	0.033	559.47	Lipids and lipid-like molecules
M778T39_1	[M − H]-	1,2-distearoyl-*sn*-glycero-3-phospho-(1′-rac-glycerol)	1.56	1.48	0.045	777.55	Lipids and lipid-like molecules
M304T126_2	[M]+	Benzalkonium chloride (c12)	29.34	0.004	0.0003	304.30	Benzenoids
M602T151	[M + H−C16H32O2]+	1-palmitoyl-2-oleoyl-3-linoleoyl-rac-glycerol	1.45	1.87	0.002	601.52	Lipids and lipid-like molecules
M214T105	[M+H]+	Tetradecylamine	1.58	0.07	0.003	214.25	Organic nitrogen compounds
M747T122	[M+H]+	1-hexadecyl-2-(9z-octadecenoyl)-*sn*-glycero-3-phosphocholine	3.71	2.37	0.003	746.60	Lipids and lipid-like molecules
M230T149	[M+H]+	Lauryldimethylamine oxide	2.10	0.39	0.004	230.25	Organic nitrogen compounds
M285T350	(M + NH4)+	Adenosine	2.99	0.45	0.007	285.13	Nucleosides, nucleotides, and analogues
M313T33_2	[M + H−H2O]+	1-palmitoylglycerol	2.87	1.49	0.009	313.27	Lipids and lipid-like molecules
M136T351_2	[M+H]+	DL-homocysteine	5.1887	0.4966	0.009	136.05	Organic acids and derivatives
M604T151	[M + H−H2O]+	1,2-dioleoyl-*sn*-glycerol	1.75	2.14	0.009	603.53	Lipids and lipid-like molecules
M154T350_2	[M+H]+	3-hydroxyanthranilic acid	5.60	0.47	0.010	154.06	Benzenoids
M246T243_1	[M+H]+	Isovaleryl-L-carnitine	6.08	0.66	0.012	246.17	Lipids and lipid-like molecules
M282T95	[M + H−H2O]+	Sphingosine	5.80	0.36	0.013	282.28	Organic nitrogen compounds
M114T129	(M + H−H2O)+	N-Acetyl-L-alanine	1.30	0.18	0.017	114.05	Organic acids and derivatives
M114T170	[M+H]+	Creatinine	4.24	0.53	0.020	114.07	Organic acids and derivatives
M773T119	[M+H]+	1-(1z-octadecenyl)-2-(9z-octadecenoyl)-*sn*-glycero-3-phosphocholine	2.79	2.29	0.021	772.61	Lipids and lipid-like molecules
M371T449	(M + Na)+	Inosine 5′-monophosphate (IMP)	1.11	0.38	0.023	371.04	Nucleosides, nucleotides, and analogues
M568T187	(M-H+2Na)+	1-Stearoyl-*sn*-glycerol 3-phosphocholine	3.57	0.62	0.024	568.34	
M628T34	(M + H−H2O)+	1-Stearoyl-2-arachidonoyl-*sn*-glycerol	1.27	1.71	0.024	627.53	Lipids and lipid-like molecules
M134T352_2	(M-H+2Na)+	L-Alanine	2.09	0.62	0.025	134.02	Organic acids and derivatives
M376T36_1	[M+H]+	Pipamperone	3.41	0.47	0.026	376.26	Organic oxygen compounds
M345T522	(M-2H+3Na)+	Tyr-Pro	1.02	1.30	0.027	345.09	
M227T423	[M+H]+	L-carnosine	4.56	0.13	0.029	227.11	Organic acids and derivatives
M241T441	(M + H)+	L-Anserine	3.26	0.20	0.032	241.13	Organic acids and derivatives
M393T36	[M+H]+	Chenodeoxycholate	2.57	0.50	0.032	393.28	Lipids and lipid-like molecules
M628T194	[M+H]+	2-epahpa [dmed-fahfa]	5.07	2.10	0.034	627.53	
M888T194	[M+H]+	1-stearoyl-2-arachidonoyl-*sn*-glycero-3-phospho-(1′-myo-inositol)	1.48	1.77	0.036	887.56	Lipids and lipid-like molecules
M205T260	[M+H]+	DL-tryptophan	1.29	0.54	0.036	205.09	Organoheterocyclic compounds

Table 2 (*continued*)

| ID	Adduct	Name	VIP	Fold change	P-value	m/z	SuperClass
M308T433	[M+H]+	L-glutathione, reduced	2.73	2.51	0.036	308.09	Organic acids and derivatives
M182T302_2	[M+H]+	DL-tyrosine	1.75	0.45	0.036	182.08	Organic acids and derivatives
M482T197	[M+H]+	1-stearoyl-2-hydroxy-*sn*-glycero-3-phosphoethanolamine	2.54	0.49	0.037	482.32	Lipids and lipid-like molecules
M241T417	[M+H]+	Anserine	12.41	0.13	0.039	241.13	Organic acids and derivatives
M405T402_2	[M+H]+	hydrocortisone 21-acetate	3.34	0.52	0.043	405.21	Lipids and lipid-like molecules
M136T302	[M + H–CH3O5P]+	O-phosphotyrosine	1.23	0.49	0.045	136.07	Organic acids and derivatives
M229T303	[M]+	Dl-tmap	9.11	0.19	0.045	229.15	Organic acids and derivatives
M137T172_1	[M+H]+	Hypoxanthine	16.12	0.70	0.046	137.05	Organoheterocyclic compounds
M256T36	[M + H–C18H34O2]+	N-palmitoyl-D-sphingosine	2.41	0.86	0.048	256.26	Lipids and lipid-like molecules
M119T174	[M + H–C2H5O2N]+	2-methylhippuric acid	1.45	0.75	0.049	119.03	Benzenoids
M795T141	[M+H]+	1-(1z-octadecenyl)-2-(5z,8z,11z,14z-eicosatetraenoyl)-*sn*-glycero-3-phosphocholine	6.50	1.57	0.049	794.60	Lipids and lipid-like molecules
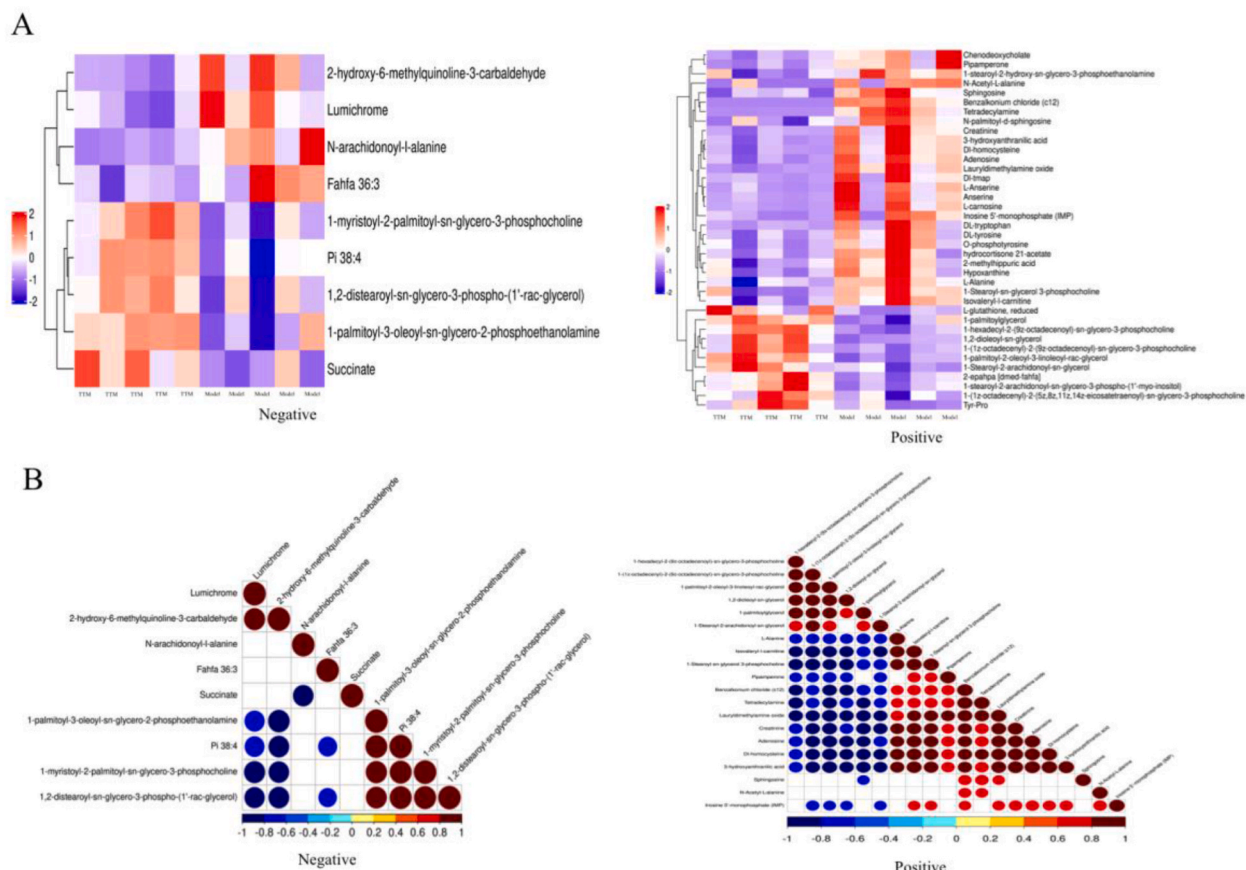
Fig. 6. Hierarchical clustering and correlation analysis of differential metabolites. (A) Hierarchical clustering analysis. The metabolites heat-map in positive and negative polarity mode. (B) Correlation analysis of metabolites with significant differences in positive and negative polarity mode.

KEGG pathway enrichment analysis result showed that differential metabolites were enriched in 66 pathways ($P < 0.05$). The top 25 were shown as Fig. 7. The detailed information of 68 pathways was seen in Table 3.

3.9. Prediction of TT's therapeutic target based on network pharmacology and metabolomics

KEGG Mapper-color tool (https://www.kegg.jp/kegg/mapper/color.html) was used to predict TT's therapeutic target according to network pharmacology and untargeted metabolomics data. The analysis result showed that 14 of 125 proteins and sphingosine were found in apoptosis signaling pathway (Fig. 8).

3.10. Effects of TT on molecules of the apoptosis signaling pathway in tumor tissues of H22 liver cancer mice

To evaluate the relationship between TT and apoptosis signaling pathway, the key protein levels were tested by Western blot. The original images were seen in supplementary results. The results were shown in Fig. 9. The levels of pro-Cathepsin B, Bax, Bax/Bcl2, and Caspase7 were significantly increased in sorafenib group, compared with model group. Moreover, the levels of pro-Cathepsin B, Cathepsin B, Bax, Bax/Bcl2, Caspase3, and Caspase7 were markedly increased after TT treatment. In addition, the level of Bcl2 was significantly reduced in TTM group compared with model group.

4. Discussion

Despite the development of new therapeutic drugs such as immune checkpoint inhibitors and targeted drugs, the mortality rate for PLC remains high due to resistance to current drugs and side effects. This highlights the urgent need for effective and affordable drugs for the treatment of PLC. TCM is an attractive option for new drug development due to its multi-target approach and relatively low cost compared to Western medicine. Anti-tumor effects of TT, one of the oldest TCM, were already verified by Shen-Nong-Ben-Cao-Jing and modern pharmacology researches [15].

In this study, transplantation tumor mouse model of liver cancer was established by H22 cell injection in infra-axillary region. After five days, tumors were observed in all mice, with tumors consistently increasing in mice from the model group. This indicated that the liver cancer mouse model was successful and reliable. And then, the anti-cancer effects of TT aqueous extract were evaluated. After 10 days of TT aqueous extract treatment, tumor size and weight were markedly decreased, tumor inhibitory rates were significantly increased. The results supported the anti-liver cancer activity of TT aqueous extract *in vivo*. In addition, tumor cellular morphology, multiplication capacity and apoptosis were respectively observed by HE and Tunel staining. The staining results showed that TT aqueous extract's anti-liver cancer action was closely related to disrupting the tight organization, inducing apoptosis and promoting adipose metaplasia.

Sphingolipids are a class of lipids that are important components of cell membranes and are involved in various cellular processes such as cell signaling, proliferation and apoptosis. Several studies have suggested that sphingolipids, including sphingosine (Sph), ceramide (Cer) and sphingosine-1-phosphate (S1P), play a role in cancer development and progression. For example, ceramide has been shown to induce apoptosis and inhibit cell proliferation, while S1P promotes cell survival and proliferation. Furthermore, Sph is able to transform into Cer and S1P via sphingoid base N-stearoyltransferase (CerS) and sphingosine kinase (SPHK). Previous studies have pointed that Sph played a special role in tumor cell death independent of Cer [16,17] and there was a closed affinity among cell cycle arrest, apoptosis and Cer [18–21]. In this study, different metabolites analysis results showed that Sph level was significantly reduced, whereas Cer level was increased in tumor tissue after TT treatment. Additionally, KEGG enrichment analysis found that Sph
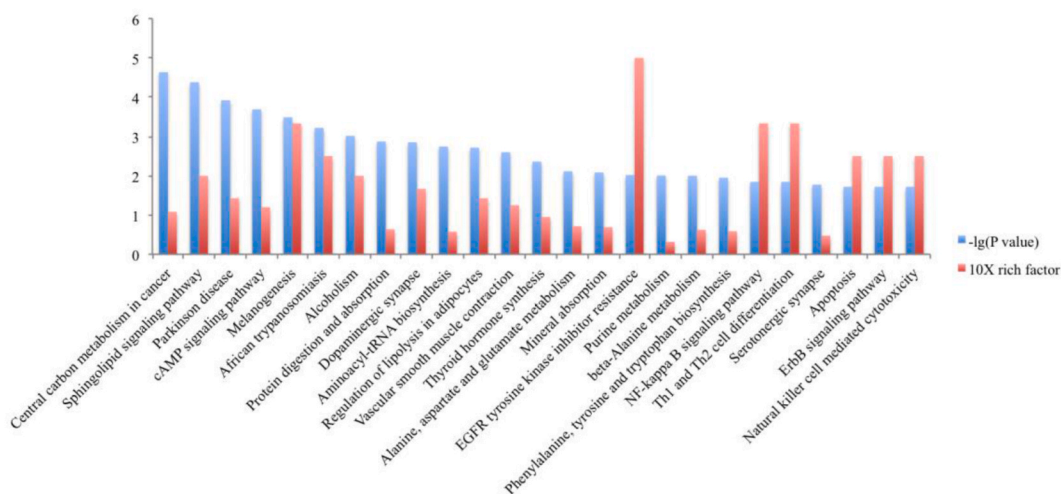

Fig. 7. KEGG enrichment analysis of differential metabolites. The top 25 of KEGG pathway enrichment analysis.

Table 3
The detailed information of KEGG pathway enrichment analysis of metabonomics.

| Pathway	Metabolite	P value
Central carbon metabolism in cancer	Succinate; L-Alanine; DL-tryptophan; DL-tyrosine	2.32E-05
Sphingolipid signaling pathway	Adenosine; Sphingosine; 1-Stearoyl-2-arachidonoyl-*sn*-glycerol	4.17E-05
Parkinson disease	Adenosine; 1-Stearoyl-2-arachidonoyl-*sn*-glycerol; DL-tyrosine	1.20E-04
cAMP signaling pathway	Succinate; Adenosine; 1-Stearoyl-2-arachidonoyl-*sn*-glycerol	2.04E-04
Melanogenesis	1-Stearoyl-2-arachidonoyl-*sn*-glycerol; DL-tyrosine	3.26E-04
African trypanosomiasis	1-Stearoyl-2-arachidonoyl-*sn*-glycerol; DL-tryptophan	6.04E-04
Alcoholism	Adenosine; DL-tyrosine	9.66E-04
Protein digestion and absorption	L-Alanine; DL-tryptophan; DL-tyrosine	1.35E-03
Dopaminergic synapse	1-Stearoyl-2-arachidonoyl-*sn*-glycerol; DL-tyrosine	1.41E-03
Aminoacyl-tRNA biosynthesis	L-Alanine; DL-tryptophan; DL-tyrosine	1.81E-03
Regulation of lipolysis in adipocytes	Adenosine; 1-Stearoyl-2-arachidonoyl-*sn*-glycerol	1.93E-03
Vascular smooth muscle contraction	Adenosine; 1-Stearoyl-2-arachidonoyl-*sn*-glycerol	2.53E-03
Thyroid hormone synthesis	1-Stearoyl-2-arachidonoyl-*sn*-glycerol; L-glutathione, reduced	4.37E-03
Alanine, aspartate and glutamate metabolism	Succinate; L-Alanine	7.70E-03
Mineral absorption	L-Alanine; DL-tryptophan	8.25E-03
EGFR tyrosine kinase inhibitor resistance	1-Stearoyl-2-arachidonoyl-*sn*-glycerol	9.59E-03
Purine metabolism	Adenosine; Inosine 5′-monophosphate (IMP); Hypoxanthine	9.92E-03
beta-Alanine metabolism	L-carnosine; L-Anserine;	9.99E-03
Phenylalanine, tyrosine and tryptophan biosynthesis	DL-tryptophan; DL-tyrosine	1.12E-02
NF-kappa B signaling pathway	1-Stearoyl-2-arachidonoyl-*sn*-glycerol	1.44E-02
Th1 and Th2 cell differentiation	1-Stearoyl-2-arachidonoyl-*sn*-glycerol	1.44E-02
Serotonergic synapse	1-Stearoyl-2-arachidonoyl-*sn*-glycerol; DL-tryptophan	1.69E-02
Apoptosis	Sphingosine	1.91E-02
ErbB signaling pathway	1-Stearoyl-2-arachidonoyl-*sn*-glycerol	1.91E-02
Natural killer cell mediated cytotoxicity	1-Stearoyl-2-arachidonoyl-*sn*-glycerol	1.91E-02
Th17 cell differentiation	1-Stearoyl-2-arachidonoyl-*sn*-glycerol	1.91E-02
T cell receptor signaling pathway	1-Stearoyl-2-arachidonoyl-*sn*-glycerol	1.91E-02
B cell receptor signaling pathway	1-Stearoyl-2-arachidonoyl-*sn*-glycerol	1.91E-02
Growth hormone synthesis, secretion and action	1-Stearoyl-2-arachidonoyl-*sn*-glycerol	1.91E-02
Glioma	1-Stearoyl-2-arachidonoyl-*sn*-glycerol	1.91E-02
PD-L1 expression and PD-1 checkpoint pathway in cancer	1-Stearoyl-2-arachidonoyl-*sn*-glycerol	1.91E-02
Histidine metabolism	L-carnosine; L-Anserine	2.09E-02
Biosynthesis of amino acids	L-Alanine; DL-tryptophan; DL-tyrosine	2.21E-02
MAPK signaling pathway	1-Stearoyl-2-arachidonoyl-*sn*-glycerol	2.38E-02
Rap1 signaling pathway	1-Stearoyl-2-arachidonoyl-*sn*-glycerol	2.38E-02
Chemokine signaling pathway	1-Stearoyl-2-arachidonoyl-*sn*-glycerol	2.38E-02
Neurotrophin signaling pathway	1-Stearoyl-2-arachidonoyl-*sn*-glycerol	2.38E-02
Kaposi sarcoma-associated herpesvirus infection	1-Stearoyl-2-arachidonoyl-*sn*-glycerol	2.38E-02
Human immunodeficiency virus 1 infection	1-Stearoyl-2-arachidonoyl-*sn*-glycerol	2.38E-02
ABC transporters	Adenosine; L-Alanine; L-glutathione, reduced	2.64E-02
VEGF signaling pathway	1-Stearoyl-2-arachidonoyl-*sn*-glycerol	2.85E-02
GnRH signaling pathway	1-Stearoyl-2-arachidonoyl-*sn*-glycerol	2.85E-02
Relaxin signaling pathway	1-Stearoyl-2-arachidonoyl-*sn*-glycerol	2.85E-02
Human cytomegalovirus infection	1-Stearoyl-2-arachidonoyl-*sn*-glycerol	2.85E-02
Non-small cell lung cancer	1-Stearoyl-2-arachidonoyl-*sn*-glycerol	2.85E-02
Phenylalanine metabolism	Succinate; DL-tyrosine	3.29E-02
Ras signaling pathway	1-Stearoyl-2-arachidonoyl-*sn*-glycerol	3.32E-02
Long-term potentiation	1-Stearoyl-2-arachidonoyl-*sn*-glycerol	3.32E-02
Adipocytokine signaling pathway	1-Stearoyl-2-arachidonoyl-*sn*-glycerol	3.32E-02
Spinocerebellar ataxia	1-Stearoyl-2-arachidonoyl-*sn*-glycerol	3.32E-02
Cocaine addiction	DL-tyrosine	3.32E-02
Cysteine and methionine metabolism	L-Alanine; L-glutathione, reduced	3.60E-02
Morphine addiction	Adenosine	3.79E-02
Fc gamma R-mediated phagocytosis	1-Stearoyl-2-arachidonoyl-*sn*-glycerol	3.79E-02
Glutamatergic synapse	1-Stearoyl-2-arachidonoyl-*sn*-glycerol	3.79E-02
Estrogen signaling pathway	1-Stearoyl-2-arachidonoyl-*sn*-glycerol	3.79E-02
Endocrine and other factor-regulated calcium reabsorption	1-Stearoyl-2-arachidonoyl-*sn*-glycerol	3.79E-02
GABAergic synapse	Succinate	4.25E-02
Apelin signaling pathway	1-Stearoyl-2-arachidonoyl-*sn*-glycerol	4.25E-02
Circadian entrainment	1-Stearoyl-2-arachidonoyl-*sn*-glycerol	4.25E-02
Long-term depression	1-Stearoyl-2-arachidonoyl-*sn*-glycerol	4.25E-02
GnRH secretion	1-Stearoyl-2-arachidonoyl-*sn*-glycerol	4.25E-02
AGE-RAGE signaling pathway in diabetic complications	1-Stearoyl-2-arachidonoyl-*sn*-glycerol	4.25E-02
Amphetamine addiction	DL-tyrosine	4.25E-02
cGMP-PKG signaling pathway	Adenosine	4.71E-02
Necroptosis	Sphingosine	4.71E-02
Adrenergic signaling in cardiomyocytes	1-Stearoyl-2-arachidonoyl-*sn*-glycerol	4.71E-02
Parathyroid hormone synthesis, secretion and action	1-Stearoyl-2-arachidonoyl-*sn*-glycerol	4.71E-02
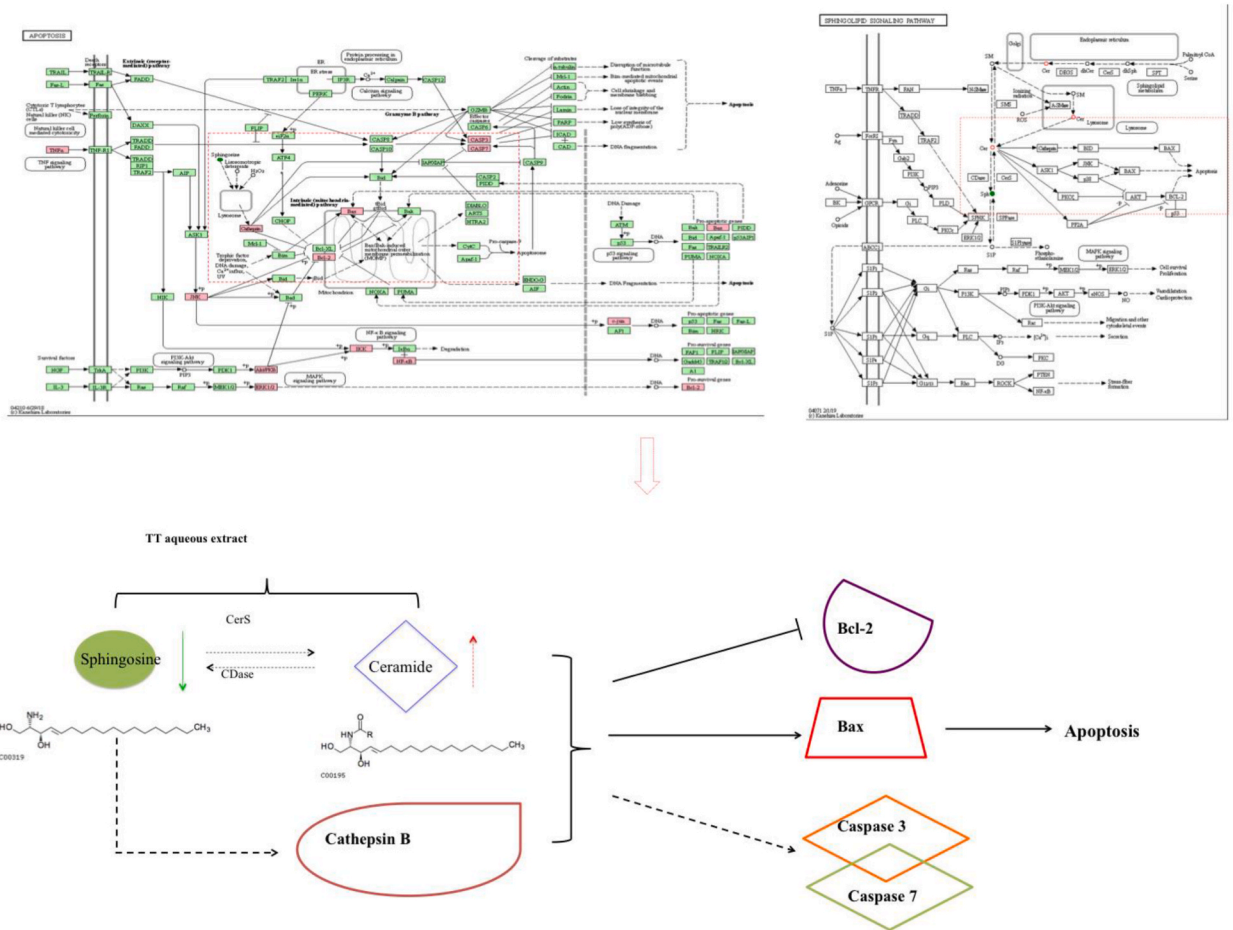
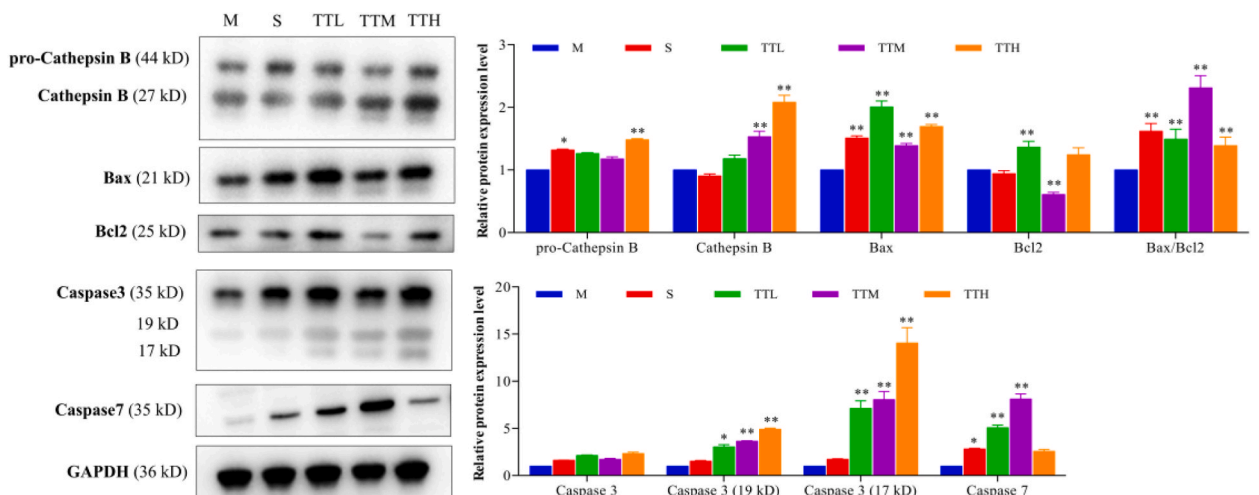**Fig. 8.** Descriptive and correlational analysis between Sph and apoptosis induced by TT.

Fig. 9. Effects of TT on the molecules of apoptosis signaling pathway in liver cancer tissue. Values given are the mean ± SEM. N = 3, *$P < 0.05$, **$P < 0.01$ versus model group. Statistical significant differences were determined using a one-way ANOVA followed by Dunnett's multiple comparisons test or post hoc analysis. The original images were seen in supplementary results.

was gathered in the apoptosis signaling pathway. Thus these data suggest that TT-induced liver cancer cell apoptosis could be resulted from reducing Sph level.

Cathepsins are a family of cysteine proteases that are involved in various cellular processes such as protein degradation, antigen presentation and apoptosis. There are 11 members in human, including cathepsin B and cathepsin D. Both cathepsin B and cathepsin D have been implicated in cancer development and progression, and activated in lysosome. Cathepsin B is a cysteine protease and downstream of Sph. A number of studies demonstrated that cathepsin B is involved in regulating cell proliferation, invasion, immune resistance and apoptosis [22–25]. Cathepsin D is an aspartic acid lysosome endopeptidase and the downstream of Cer. It has been shown that cathepsin D is also involved in apoptosis, proliferation and angiogenesis [26–28].

In this study, the level of Sph in tumor tissue was determined by metabolomics, and then the downstream proteins of Sph in apoptosis signaling pathway were assessed. The results revealed that tumor cell apoptosis was induced by TT aqueous extract.

5. Conclusions

TT aqueous extract efficaciously inhibited tumor growth, induced tumor cell damage, and promoted apoptosis. In addition, the activation of the apoptosis signaling pathway by reducing Sph level was identified as one of the molecular mechanisms of TT in liver cancer. This study provides a preliminary pharmacological basis for the use of TT in treating liver cancer. However, it is important to note that further research is needed to validate other potential therapeutic targets and to fully understand the mechanism through which TT may exert its effects on these targets. Nonetheless, the use of network pharmacology and untargeted metabolomics data provided a promising approach for identifying potential therapeutic targets of TCM.

Author contribution statement

Jing Zhao: Performed the experiments; Analyzed and interpreted the data; Contributed reagents, materials, analysis tools or data; Wrote the paper.

Jia-Qi Zhang; Tan-Tan Li: Performed the experiments.

Sen Qiao: Conceived and designed the experiments; Contributed reagents, materials, analysis tools or data.

Shu-Long Jiang: Conceived and designed the experiments; Contributed reagents, materials, analysis tools or data; Wrote the paper.

Data availability statement

Data will be made available on request.

Declaration of competing interest

The authors declare that they have no competing interests.

Acknowledgments

List of abbreviations

IARC (International Agency for Research on Cancer); PLC (primary liver cancer); TCM (traditional Chinese medicine); TT (*Tribulus terrestris* L.); TCMSP (Traditional Chinese Medicine Systems Pharmacology); OB (oral bioavailability); DL (drug-likeness); PPI (protein-protein interaction); GO (gene ontology); KEGG (Kyoto Encyclopedia of Genes and Genomes); HE (hematoxylin and eosin); BP (biological processes); MF (molecular function); CC (cellular component); Cer (ceramide); Sph (sphingosine); S1P (sphingosine-1-phosphate); CerS (sphingoid base N-stearoyltransferase); SPHK (sphingosine kinase).

Appendix A. Supplementary data

Supplementary data to this article can be found online at https://doi.org/10.1016/j.heliyon.2023.e17612.

References

[1] C.P. Wild, E. Weiderpass, B.W. Stewart, World Cancer Report, Cancer Research for Cancer Prevention, Lyon, France, 2020, pp. 355–366.

[2] X. Tang, L. Ge, Z. Chen, et al., Methylation of the constitutive androstane receptor is involved in the suppression of CYP2C19 in hepatitis B Virus–associated hepatocellular carcinoma, Drug Metab. Dispos. 44 (10) (2016) 1643–1652.

[3] J.-M. Hu, K.-C. Liu, J. Luo, HIV-HBV and HIV-HCV coinfection and liver cancer development, Cancer Treat Res. 177 (2019) 231–250.

[4] Y. Liu, C.-C. Chang, G.M. Marsh, et al., Population attributable risk of aflatoxin-related liver cancer: systematic review and meta-analysis, Eur. J. Cancer 48 (14) (2012) 2125–2136.

[5] Y.-Y. Fan, X.-W. Hou, P.-P. Guo, et al., Extraction of *Amana edulis* induces liver cancer apoptosis, Evid. Based Complement Alternat. Med. 4 (2018), 3927075.

[6] J.-H. Chen, S.H. Kim, P.-W. Fan, et al., The aqueous extract of Chinese medicinal herb *Brucea javanica* suppresses the growth of human liver cancer and the derived stem-like cells by apoptosis, Drug Des. Devel. Ther 17 (10) (2016) 2003–2013.

[7] L.-P. You, X.-N. Kong, Q.-Y. Gao, et al., 基于文献的中药治疗肝癌实验研究现状分析, J. Tradit. Chin. Med. 64 (1) (2023) 77–82.

[8] H.O. Santos, S. Howell, F.J. Teixeira, Beyond tribulus (*Tribulus terrestris* L.): the effects of phytotherapics on testosterone, sperm and prostate parameters, J. Ethnopharmacol. 235 (2019) 392–405.

[9] A.V. Sirotkin, A. Kolesárová, Puncture vine (*Tribulus Terrestris* L.) in control of health and reproduction, Physiol. Res. 70 (Suppl4) (2021) s657–s667.

[10] H.-J. Pei, J. Yang, F.-X. Hu, et al., *Tribulus terrestris L.* protects glomerular endothelial cells via the miR155-H2AC6 interaction network in hypertensive renal injury, Ann. Transl. Med. 9 (21) (2021) 1626.

[11] A.V. Sirotkin, R. Alexa, A.H. Harrath, Puncturevine (*Tribulus terrestris* L.) affects the proliferation, apoptosis, and ghrelin response of ovarian cells, Reprod. Biol. 20 (1) (2020) 33–36.

[12] J. Chen, X.-L. Bian, F.-Y. Zhu, et al., Investigation on Traditional Chinese Medicine syndrome elements and symptom distribution of liver cancer, J. Oncol. Chin. Med. 4 (2) (2022) 47–50.

[13] L.L. Sara, P.J. Harish, M.T. Chinmay, Histone deacetylase 3 coordinates deacetylase-independent epigenetic silencing of transforming growth factor-β1 (TGF-β1) to orchestrate second heart field development, J. Biol. Chem. 290 (2015) 27067–27089.

[14] J. Zhao, Y.C. Chan, B. He, et al., A patent herbal drug Yi-Shen-Hua-Shi granule ameliorates C-BSA-induced chronic glomerulonephritis and inhabits TGFβ signaling in rats, J. Ehnopharmacol. 236 (2019) 258–262.

[15] M. Dai, Y. Cao, Z.Y. Yu, Shen-Nong-Ben-Cao-Jing, Guangxi Science and Technology, Publishing House, 2016.

[16] O. Cuvillier, Sphingosine in apoptosis signaling, Biochim. Biophys. Acta 1585 (2002) 153–162.

[17] T.A. Taha, T.D. Mullen, L.M. Obeid, A house divided: ceramide, sphingosine, and sphingosine-1-phosphate in programmed cell death, Biochim. Biophys. Acta 1758 (12) (2006) 2027–2036.

[18] P. Grbčić, E.P.M. Car, M. Sedić, Targeting ceramide metabolism in hepatocellular carcinoma: new points for therapeutic intervention, Curr. Med. Chem. 27 (39) (2020) 6611–6627.

[19] M.L. Berwick, B.A. Dudley, K. Maus, et al., The Role of Ceramide 1-Phosphate in inflammation, cellular proliferation, and wound healing, Adv. Exp. Med. Biol. 1159 (2019) 65–77.

[20] M. Colombini, Ceramide channels and their role in mitochondria-mediated apoptosis, Biochim. Biophys. Acta 1797 (6–7) (2010) 1239–1244.

[21] M. Aslan, E. Afşar, E. Kırımlıoglu, et al., Antiproliferative effects of thymoquinone in MCF-7 breast and HepG2 liver cancer cells: possible role of ceramide and ER stress, Nutr. Cancer 73 (3) (2021) 460–472.

[22] O. Mijanović, A. Branković, A.N. Panin, et al., Cathepsin B: a sellsword of cancer progression, Cancer Lett. 449 (2019) 207–214.

[23] C. Chen, M.J. Ahmad, T. Ye, et al., Cathepsin B regulates mice granulosa cells' apoptosis and proliferation in Vitro, Int. J. Mol. Sci. 22 (21) (2021), 11827.

[24] W. Bao, Q. Fan, X. Luo, et al., Silencing of Cathepsin B suppresses the proliferation and invasion of endometrial cancer, Oncol. Rep. 30 (2) (2013) 723–730.

[25] B. Bian, S. Mongrain, S. Cagnol, et al., Cathepsin B promotes colorectal tumorigenesis, cell invasion, and metastasis, Mol. Carcinog. 55 (5) (2016) 671–687.

[26] C.F. Sales, R.M.C. Melo, A.P.B. Pinheiro, et al., Autophagy and Cathepsin D mediated apoptosis contributing to ovarian follicular atresia in the Nile tilapia, Mol. Reprod. Dev. 86 (11) (2019) 1592–1602.

[27] G. Berchem, M. Glondu, M. Gleizes, et al., Cathepsin-D affects multiple tumor progression steps in vivo: proliferation, angiogenesis and apoptosis, Oncogene 21 (38) (2002) 5951–5955.

[28] N.-N. Wang, H.-Z. Liu, G.-J. Liu, et al., Yeast β-D-glucan exerts antitumour activity in liver cancer through impairing autophagy and lysosomal function, promoting reactive oxygen species production and apoptosis, Redox Biol. 32 (2020), 101495.